ELSEVIER

Inorganica Chimica Acta 226 (1994) 43–51

Inorganica Chimica Acta

The electronic structure of pentaammine(pyrazine) ruthenium(II) and (III): the metal–ligand π conjugation and its implications in electron delocalization

Li-Tai Zhang [a], Mary Jo Ondrechen [b,1]

[a] *Department of Chemistry, Pomona College, Claremont, CA 91711, USA*

[b] *Department of Chemistry, Northeastern University, Boston, MA 02115, USA; Kemisk Institut, Århus Universitet, DK-8000 Århus C, Denmark*

Received 25 February 1994

Abstract

Results of electronic structure calculations on the title cations are reported. Our transition operator calculations have confirmed the original assignments of optical absorption transitions at 250 and 470 nm for the 2+ ion and have suggested assignments for transitions observed at 238 and 270 nm for the 3+ ion. Because the pyrazine ligand resides in an asymmetric environment, the identities and symmetry designations of the six π states of the free ligand are heavily obscured in these cations. The 2+ species exhibits substantial mixing of the Ru $4d_{xz}$ orbital with a π^* orbital of pyrazine, while the 3+ species does not. Conversely the 3+ ion shows some mixing of the $4d_{xz}$ orbital with a π orbital of pyrazine, while the 2+ ion has only weak mixing of these orbitals. We find that the polarization of the pyrazine ligand is toward the metal ion, which is consistent with simple electrostatic predictions. The dependence of the π-bonding and backbonding strengths upon the electron occupation (or charge) of the metal species is an important feature of the ruthenium–pyrazine system. The electron density distribution within the pyrazine ligand also depends strongly on the charge. Implications for extended and complexed mixed-valence species are discussed.

Keywords: Electronic structures; Electronic delocalization; Ruthenium complexes; Ammine complexes; Pyrazine complexes

1. Introduction

The backbonding capability of the Ru^{2+} ion is a significant feature of the chemistry of ruthenium [1,2]. It plays an important role in electron delocalization in widely investigated ruthenium mixed-valence compounds such as the Creutz–Taube ion [3–10], and their corresponding oligomers [11,12] and higher polymers [13].

In the present paper we examine metal–ligand bonding in the π-electron system of the ruthenium–pyrazine system, and report the electronic structure of the pentaamine(pyrazine) ruthenium(II) and (III) cations [14–17]. We use the Hartree–Fock Slater discrete variational method (HFS-DVM), which has been applied successfully to the Creutz–Taube ion, the valence-averaged dimeric analogue of the present species. The HFS-DVM predicts correctly or is consistent with all of the observed spectroscopic properties of that dimer complex [7]. One of the main goals of the present work is to understand more thoroughly the interaction between ruthenium and π-accepting ligands, and to achieve thereby a greater understanding of extended complexes containing more than one metal ion. Very recently Hupp and co-workers [18,19] reported intriguing spectral changes in the Creutz–Taube ion and related bridged species upon asymmetric crown-ether complexation. Information about the ruthenium–pyrazine interaction in an asymmetric environment may help in the interpretation of those observations.

In the dimeric mixed-valence complexes, where two ruthenium ions are joined together by a bridging ligand, the observed properties of the complex and the degree of metal–metal interaction are strongly dependent on the electronic structure of the bridging ligand [20,21]. Furthermore, extended chains of metal ions (M) and bridging ligands (L) with the linear structure ...M–L–M–L–M... have been synthesized [11,13]. Such compounds may have important applications, because

[1] On sabbatical leave at Aarhus University through March 1994. Permanent address: Northeastern University.

SSDI 0020-1693(94)04069-8

of the possibility of conductivity along the M–L axis, but more significantly, because of the possibility of control of the conductive properties through chemical substitution on the bridging ligand. In the present work, we focus exclusively on the monomeric species M–L. We wish to understand the fundamental backbonding interaction between M and L, with particular attention to the dependence of this interaction upon the electron occupation, and to the distribution of electrons in the bridging ligand in an asymmetric environment.

In the next section our electronic structure method is reviewed briefly. In Section 3 the input data are discussed. The results of the ground states of the complexes of interest are presented in Section 4. Transition state results and optical absorption transitions are given in Section 5. Comments on the recent asymmetrically complexed systems of Hupp and co-workers are given in Section 6 and we conclude with Section 7.

2. Method

The HFS-DVM has been applied extensively to both organometallic ions and molecules [22–25]. The DVM is one method for solving the HFS equations without invoking the muffin-tin approximation [26]. It is a first-principles, non-empirical method. We utilize the spin-polarized one-electron local density model, the Hamiltonian for which is given by:

$$\hat{H}_\mu = \hat{T} + \hat{V}_c + \hat{V}_{x,\mu} \quad (1)$$

where μ is a spin index ($\uparrow$ or $\downarrow$), $\hat{T}$ and $\hat{V}_c$ are the kinetic energy and Coulomb potential operators, and $\hat{V}_{x,\mu}$ is the exchange and correlation potential for an electron with spin μ, given by:

$$\hat{V}_{x,\mu} = -3X_\alpha(3\rho_\mu/4\pi)^{1/3} \quad (2)$$

where X_α is a scaling constant, with $2/3 < X_\alpha < 1$. The exchange-correlation potential depends on the spin density ρ_μ, which is taken to be a linear combination of single particle contributions as:

$$\rho_\mu(r) = \sum_n f_{n\mu}|\psi_{n\mu}(r)|^2 \quad (3)$$

Here $f_{n\mu}$ is an occupation number and $\psi_{n\mu}$ is an eigenfunction of $\hat{H}_\mu$. This scheme (Eqs. 1–3) is solved self-consistently. The molecular wavefunctions are expanded in the usual LCAO fashion as:

$$\psi_{n\mu} = \sum_j C_{n\mu j}\phi_j \quad (4)$$

where the ϕ_i are symmetry adapted linear combinations of atomic orbitals. The atomic orbitals (AOs) are obtained numerically using an HFS-SCF procedure on the atoms. The elements of the Hamiltonian and overlap matrices are obtained by direct numerical integration, employing a diophantine integration method [27,28].

3. Input data

For the geometry of the two ruthenium pyrazine monomers we used the crystallographic data of Gress et al. [16]. The point-group of the ions is C_s, with a mirror in the xz plane. X_α was taken to be 0.7, which has been shown to be the optimal value for a variety of molecules and materials [29]. Here z is the Ru–N(pyz) axis, and the y axis lies in the pyz plane. Bond distances and basis sets used for the calculations on the complexes are summarized in Table 1.

4. Ground-state results

Energies and symmetries for molecular orbitals lying near the highest occupied molecular spin orbital (HOMSO) and the lowest unoccupied molecular spin orbital (LUMSO) are given in Tables 2 and 3. Energies (in eV) are given for the converged ground states of the complexes. The symmetry designation is given for each MO in C_{2v}. (This is the molecular point group if the H atoms on NH_3 are ignored.) The symmetry designation is also given in the point group C_s. (C_s is the symmetry of the ions if the H atoms on NH_3 are not ignored and is the symmetry used in these calculations.) A′ and A″ designate the two irreducible representations in the point group C_s. The spin state is designated by + or −. Since Koopmans' theorem is not obeyed in the local density model, we regard as significant the energy *differences* between the converged ground-state spin orbitals; the absolute energies are less meaningful. The LUMSO and HOMSO are 1.9 eV apart for the Ru^{2+} monomer. For the Ru^{3+} monomer they are calculated to be only 0.02 eV apart, which is

Table 1
Internuclear distances (Å) and basis set

	(II)	(III)
Ru–N(pyz)	2.006	2.076
Ru–N(*cis*)	2.152	2.106
Ru–N(*trans*)	2.166	2.125

Basis set

1s on H
1s, 2s, 2p on C
1s, 2s, 2p on N
1s–6s, 2p–5p, 3d–4d on Ru

With the following core functions frozen:

1s on C and N
1s–3s, 2p–3p, 3d on Ru

Table 2
Molecular spin orbital energies and symmetries for $[Ru(NH_3)_5pyz]^{2+}$

Spin orbital[a] (in C_s)	Energy (in eV)	Symmetry (in C_{2v})	Main components[b]
26A′−	−5.61	B_1	π^*[MO#6, Fig. 2]
29A′+	−5.61	B_1	π^*[MO#6, Fig. 2]
18A″−	−9.04	B_2	π^*[MO#5, Fig. 2]
18A″+	−9.04	B_2	π^*[MO#5, Fig. 2]
26A′−	−9.81	B_1	π^*[MO#4, Fig. 2]; some $4d_{xz}$
26A′+	−9.81	B_1	π^*[MO#4, Fig. 2]; some $4d_{xz}$
25A′−	−11.72	A_1	$4d_{x2-y2}$
25A′+	−11.72	A_1	$4d_{x2-y2}$
17A″+	−11.85	B_2	$4d_{yz}$
17A″−	−11.85	B_2	$4d_{yz}$
24A′+	−11.88	B_1	$4d_{xz}$; some π^* [MO#4, Fig. 2]
24A′−	−11.88	B_1	$4d_{xz}$; some π^* [MO#4, Fig. 2]
16A″−	−14.90	B_2	π[MO#3, Fig. 2]
16A″+	−14.90	B_2	π[MO#3, Fig. 2]
22A′−	−15.07	B_1	π[MO#2, Fig. 2]
22A′+	−15.07	B_1	π[MO#2, Fig. 2]
19A′+	−17.51	B_1	π[MO#1, Fig. 2]
19A′−	−17.51	B_1	π[MO#1, Fig. 2]

[a]Spin orbitals below the gap are occupied.
[b]See Figs. 2 and 3 for sketches.

Table 3
Molecular spin orbital energies and symmetries for $[Ru(NH_3)_5pyz]^{3+}$

Spin orbital[a] (in C_s)	Energy (in eV)	Symmetry (in C_{2v})	Main components[b]
29A′+	−9.86	B_1	π^*[MO#6, Fig. 2]
29A′−	−9.87	B_1	π^*[MO#6, Fig. 2]
19A″+	−13.49	A_2	π^*[MO#5, Fig. 2]
18A″−	−13.50	A_2	π^*[MO#5, Fig. 2]
26A′−	−14.39	B_1	π^*[MO#4, Fig. 2]; some d_{xz}
26A′+	−14.44	B_1	π^*[MO#4, Fig. 2]; some d_{xz}
25A′−	−16.95	A_1	$4d_{x2-y2}$
24A′−	−16.97	B_1	$4d_{xz}$
17A″−	−17.08	B_2	$4d_{yz}$
24A′+	−17.70	B_1	$4d_{xz}$
23A′+	−17.79	A_1	$4d_{x2-y2}$
17A″+	−17.91	B_2	$4d_{yz}$
16A″−	−19.17	A_2	π[MO#3, Fig. 2]
16A″+	−19.17	A_2	π[MO#3, Fig. 2]
22A′−	−19.58	B_1	π[MO#2, Fig. 2]; some d_{xz}
22A′+	−19.62	B_1	π[MO#2, Fig. 2]; some d_{xz}
20A′−	−21.61	B_1	π[MO#1, Fig. 2]
20A′+	−21.63	B_1	π[MO#1, Fig. 2]

[a]Spin orbitals below the gap are occupied.
[b]See Figs. 2 and 3 for sketches.

less than the accuracy of the method and is therefore taken with caution. The second lowest unoccupied molecular spin orbitals are about 2.5 eV higher in energy than the LUMSO in the 3+ species.

Basis set expansion coefficients (LCAO coefficients) for selected molecular orbitals of the converged ground states of the two monomers are given in Tables 4 and 5. Fig. 1 shows the atom numbering scheme.

In an earlier paper on the electronic structure of the Creutz–Taube ion, the original assumption [3] that the two Ru ions are backbonded to an empty π^* orbital on the pyrazine ring was confirmed by us [7]. This π^*

Table 4
LCAO coefficients for selected molecular orbitals in $[Ru(NH_3)_5pyz]^{2+}$

	$4d_{xz}$	$2p_x$			
	Ru	C^{5+6} [a]	C^{7+8} [a]	N^3_{pyz}	N^4_{pyz}
19A′	0.093	0.597	0.319	0.501	0.121
22A′	0.077	0.174	−0.730	0.548	−0.324
16A″		−0.760	−0.650		
24A′	−0.800	0.511	−0.023	−0.096	0.296
26A′	−0.316	−0.561	−0.332	0.515	0.459
18A″		0.678	−0.735		
29A′	−0.051	−0.598	0.680	0.260	−0.346
25A′	−0.993	$4d_{x2-y2}$			
17A″	0.989	$4d_{yz}$			
19A″	0.960	$4d_{xy}$			
28A′	0.954	$4d_{z2}$			

[a]This is a sum combination of $2p_x$ orbitals in the A′ representation and a difference combination in the A″ representation.

Table 5
LCAO coefficients for selected molecular orbitals in $[Ru(NH_3)_5pyz]^{3+}$

	$4d_{xz}$	$2p_x$			
	Ru	C^{5+6} [a]	C^{7+8} [a]	N^3_{pyz}	N^4_{pyz}
20A′+	−0.092	0.442	0.234	0.359	0.102
22A′+	−0.256	−0.022	0.741	−0.461	0.504
16A″+		0.797	0.604		
24A′+	0.885	−0.364	0.148	−0.094	0.230
26A′+	−0.160	−0.675	−0.258	0.515	0.432
19A″+		0.628	−0.778		
29A′+	−0.029	−0.554	0.700	0.226	−0.375
20A′−	0.072	0.438	0.237	0.351	0.103
22A′−	−0.180	−0.054	0.749	−0.480	0.517
16A″−		0.797	0.604		
24A′−	−0.871	0.403	−0.077	−0.007	−0.222
26A′−	−0.207	−0.661	−0.264	0.516	0.429
18A″−		0.632	−0.774		
29A′−	−0.032	−0.558	0.703	0.228	−0.376
23A′+	−0.986	$4d_{x2-y2}$			
17A″+	−0.985	$4d_{yz}$			
25A′−	−0.933	$4d_{x2-y2}$			
17A″−	−0.985	$4d_{yz}$			

[a]This is a sum combination of $2p_x$ orbitals in the A′ representation and a difference combination in the A″ representation.

orbital may be represented by the orbital number 4 in Fig. 2. In the bridged dimer, where the two termini are metal ions joined together by a bridge orbital in the middle, the three resulting molecular orbitals are bonding (B), nonbonding (N) and antibonding (A) combinations resembling the Hückel MOs of the allyl π system (see Fig. 3 of Ref. [7]). In the case of the Creutz–Taube ion, the bridge orbital contained in the B and A combinations is the π^* orbital mentioned above. In addition, the mostly purely metallic nonbonding orbital of the Creutz–Taube ion contains a very small amount of one pyrazine π orbital which can be represented by the orbital number 2 in Fig. 2. In Ref. [13], Creutz and Chou suggest that there may be compensating π-bonding (ligand to metal donation) and backbonding (metal to ligand donation) interactions. From their solvent-dependent studies of the spectra of the monomers as well as dimeric complexes, they infer that the metal 4d orbitals interact strongly with both the π and the π^* orbitals mentioned above.

Upon examination of the LCAO coefficients one finds that, because the pyrazine ring no longer possesses D_{2h} symmetry, the π and π^* orbitals do not appear in the ruthenium pyrazine monomers with the same identities and symmetries as they did in the symmetrical Creutz–Taube ion. The molecular orbitals of the monomers which contain the Ru $4d_{xz}$ orbitals and the $p\pi$ orbitals of pyrazine resemble the Hückel benzyl

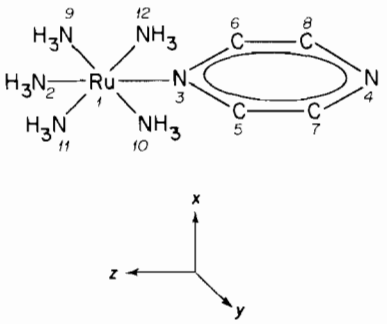

Fig. 1. The atom numbering scheme of $[Ru(NH_3)_5pyz]^{2+}$ and $[Ru(NH_3)_5pyz]^{3+}$ used in the present calculation.

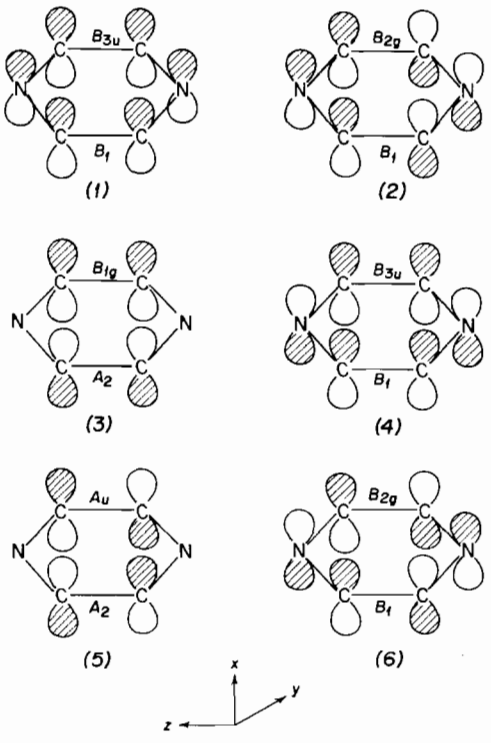

Fig. 2. A schematic diagram of the MOs of the pyrazine molecule.

system. These MOs are shown schematically in Fig. 3. We see that the molecular orbital 22A′ is in some sense a bonding combination of the Ru $4d_{xz}$ orbital and the π orbital (MO #2 of Fig. 2) of pyrazine for the 3+ monomer, but the ring π part of the orbital does not possess the plane of symmetry which bisects

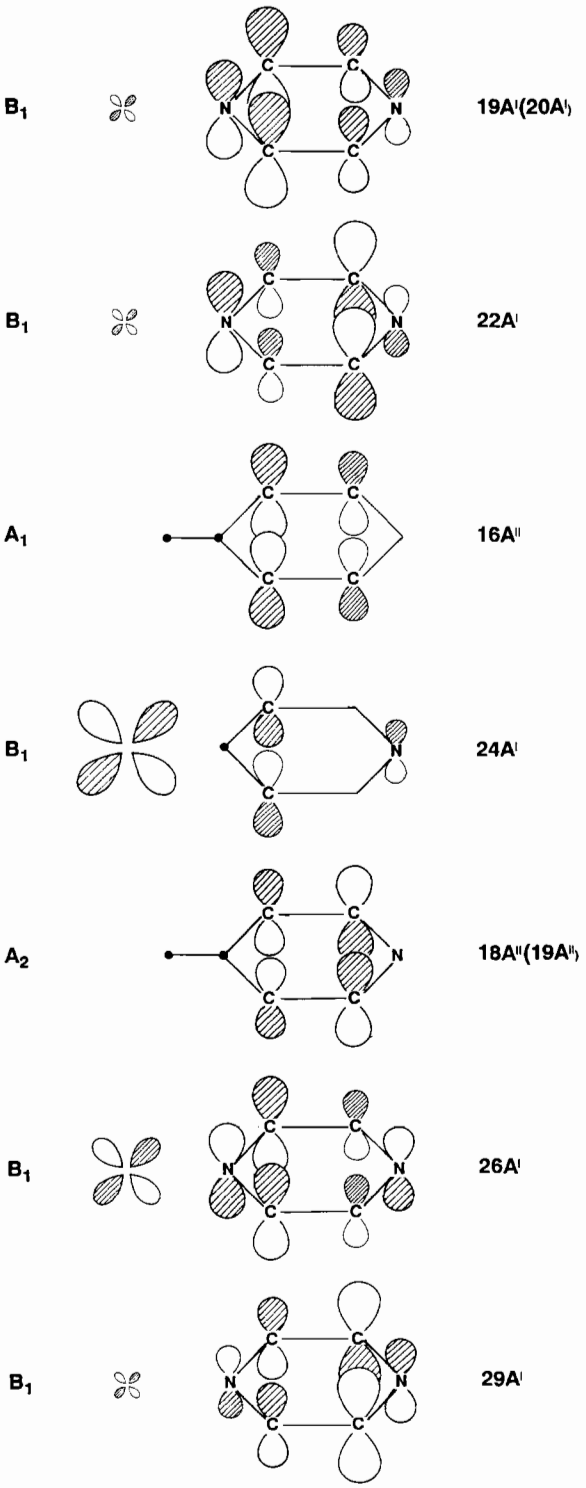

Fig. 3. A schematic diagram of the seven π molecular orbitals of the ruthenium–pyrazine system.

the two C–C bonds of pyrazine. (For the 2+ monomer 22A′ is almost entirely the pyz π MO #2 of Fig. 2, only with lowered symmetry.) The molecular orbital 26A′ (a B_1 orbital shown in Fig. 3) may be viewed as an antibonding combination of the Ru $4d_{xz}$ and the π^* orbital (MO #4 of Fig. 2) discussed above. Molecular orbital 24A′, with a bit of a stretch of the imagination, also might be thought of as a bonding combination of $4d_{xz}$ and π^*, or alternatively as an antibonding combination of $4d_{xz}$ and π.

The LCAO coefficients for 22A′ and 26A′ appear to support the suggestion of Creutz and Chou [17]: one finds greater mixing of Ru $4d_{xz}$ and the π in the 3+ complex than in the 2+ complex and greater mixing of Ru $4d_{xz}$ and the π^* in the 2+ complex than in the 3+ complex. The 22A′ molecular orbital is primarily π (MO #2 of Fig. 2) in character, with Ru $4d_{xz}$ coefficients of 0.256 and 0.077 for the 3+ and 2+ species, respectively. The 26A′ is primarily π^* (MO #4 of Fig. 2) in character, with Ru $4d_{xz}$ coefficients of −0.160 and −0.316 for the 3+ and 2+ species, respectively. Thus it does appear that the π-bonding and backbonding may act in a partially compensating fashion.

The above effects also give rise to the differences in energy level diagrams (Fig. 4) of the two monomers. (Note that in Fig. 4 the energy origins have been shifted for the 2+ and 3+ species. This is because in the

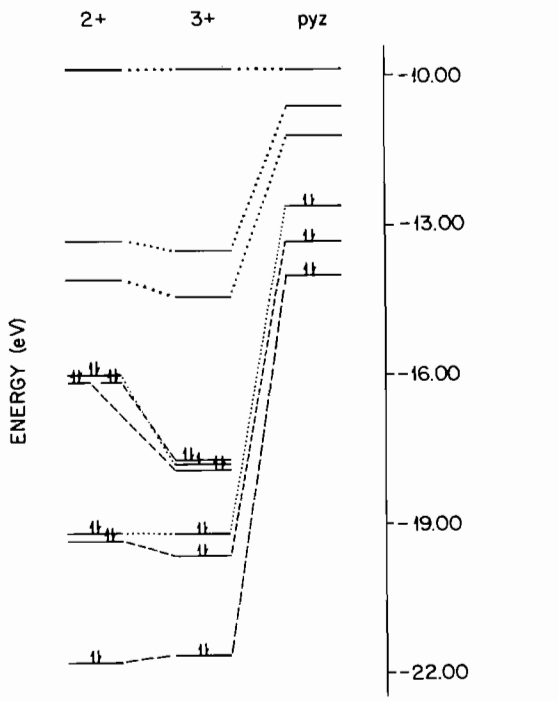

Fig. 4. Energy level diagram correlation (with energies in eV) for the converged ground state of Ru–pyrazine complexes: (1) $[Ru(NH_3)_5pyz]^{2+}$; (2) $[Ru(NH_3)_5pyz]^{3+}$ and (3) pyrazine molecule (Hückel MOs). (Origins have been shifted.) The spin–spin exchange splitting is not shown for the 3+ species.

HFS method, there is an artificial shift in the energy origin for the two species with different total charge, and therefore the absolute energies are less meaningful than the relative energies for a single complex.) For the Ru(II) monomer, the 'bonding combination of $4d_{xz}$ and π^*', 24A', is slightly lower in energy than the other two (uncoupled) t_{2g} orbitals due to the mixing with the pyrazine π^* orbital, while for Ru(III) no such effect is observed. This is apparent from analysis of the molecular energy levels of the two complexes (see Tables 2 and 3). The magnitude of the π-bonding and back-bonding between the ligand and the metal ion contributes to the splitting of the d orbitals. Both Ru(II) and Ru(III) ammines have a ligand field splitting Δ of about 3 or 4 eV, the splitting being a little larger for Ru(II). (This is based on the discussion in Ref. [1] and on the present calculations.) These energy gaps between t_{2g} and e_g are large enough so that both complexes have low-spin configuration with empty e_g orbitals [30]; see Fig. 5. To a small extent this facilitates the π interaction with pyrazine because the t_{2g} manifold is close in energy to the available, occupied orbitals in the pyrazine π system. However, for Ru(III) the t_{2g} manifold is even lower in energy because of one more positive charge, so that the energy difference between $4d_{xz}$ and π^* is large (about 3 eV in the 3+ versus about 2 eV in the 2+ species). This larger energy gap in the 3+ weakens the backbonding interaction between the two orbitals. In addition, the spatial overlap between them is expected to be weaker also, due to contraction of the 4d orbitals upon oxidation. On the other hand the difference in energy between d_{xz} and π for Ru(III) is smaller (about 2 eV) than for Ru(II) (about 3 eV). Therefore the degree of mixing between d_{xz} and π for Ru(III) is greater than for Ru(II). The stronger π-bonding in the 3+ species and the stronger backbonding in the 2+ species may also be facilitated by ligand polarization effects.

For the Ru(II) monomer the d_{xz} orbital is only slightly lower in energy than the other two orbitals in the t_{2g} manifold. The squares of the LCAO coefficients demonstrate that the $4d_{xz}$–π^*-'bonding' MO, 24A', is mainly metal in character with about 0.4 electrons in the pyrazine π^* moiety. The 'antibonding' MO, 26A', is mainly ligand in character with about 0.1 electrons in the Ru $4d_{xz}$ basis orbital. On the other hand, the Ru(III) monomer 24A', which is primarily Ru $4d_{xz}$ in character, has about 0.2 electrons in a π orbital and 26A' has only 0.03–0.04 electrons in the metal $4d_{xz}$ orbital.

If the amount of mixing of the Ru $4d_{xz}$ and the pyrazine π^* orbitals is used as a measure of the degree of backbonding strength, then the order of backbonding strength is: Creutz–Taube ion $\geq$2+ monomer > 3+ monomer. It is possible that the mixed-valence dimer has slightly stronger backbonding than the 2+ monomer because of the extra stability resulting from the ligand-

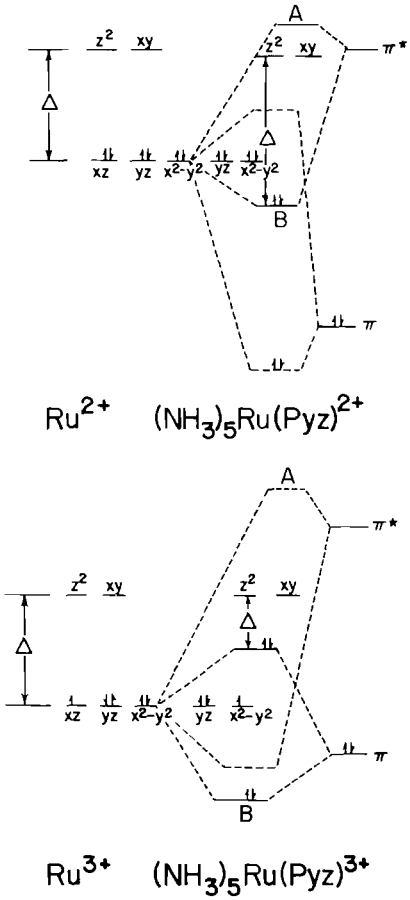

Fig. 5. Ligand-field scheme for Ru d orbitals of $[Ru(NH_3)_5pyz]^{2+}$ and $[Ru(NH_3)_5pyz]^{3+}$. Splittings are shown greatly exaggerated. The spin–spin exchange splitting is not shown for the 3+ species.

mediated mixing of the two remote Ru $4d_{xz}$ basis states in resonance. With regard to the two monomers, there is a great deal of experimental evidence that back-bonding is stronger in the 2+ complex than in the 3+ complex. For instance, the Ru–N(pyz) bond length for the Ru(II) species is shorter than for Ru(III) [16]. The basicity of the uncoordinated nitrogen on the coordinated pyrazine of Ru(II) is greatly enhanced compared to that of Ru(III) [15]. Such effects are clear from the pK_a values [15,17] of the protonated Ru(II) and Ru(III) complexes, 2.5 and −0.8, respectively. There is a very intense MLCT band for the Ru(II) complex at 470 nm which has never been reported for the Ru(III) complex.

The net Mulliken charges (obtained by summation of the Mulliken populations) for the ruthenium(II) monomer are +1.75 for Ru, −0.58 for the near N and −0.06 for the far N. This suggests that the polarization of the pyrazine ligand is toward the metal. Sun et al. [31] reported extended Hückel MO calculations (EHMO) on a series of Ru compounds, including the 2+ pyrazine monomer. They reported net atomic charges for the N atoms on the free pyrazine molecule as −1.08, −1.331 for the near N atom in the Ru(II)

pyrazine complex and −1.505 for the far N atom. Their results show an increased electron density for both nitrogen atoms of pyrazine in the $[Ru(NH_3)_5pyz]^{2+}$ complex, attributable to the backbonding interaction. However, the direction of the pyrazine dipole moment in this complex is in the direction opposite to ours. A similar discrepancy between HFS-DVM and EHMO results occurred for pentaamminedinitrogenruthenium(II) [22]. The HFS-DVM predicted that the dipole moment on the dinitrogen ligand points toward the metal ion, in agreement with experimental vibrational data [32] and with a Hartree–Fock calculation [33]. Again an EHMO calculation on analogous model species predicted a ligand dipole moment in the opposite direction [34]. The direction of the ligand polarization predicted by us for a polarizable ligand next to a positively charged ion is the one predicted by simple electrostatic arguments. Simple MO arguments predict the opposite polarization, because of a node on the near N atom in an occupied MO.

5. Transition-state results

In the HSF-DVM, the energies of optical transitions cannot be obtained with accuracy from simple subtraction of two ground state MO energies. Transition energies are properties of both initial and final electronic states. These energies were obtained using a transition state method developed by Slater [26].

In Table 6, some of the predicted transition energies and corresponding experimental data are listed. The transition observed for the Ru(II) monomer in the absorption spectrum at about 250 nm by Ford et al. [15] was previously assigned to $\pi \rightarrow \pi^*$. We find a z-polarized transition at 236 nm, which upon examination of eigenfunctions is found to be a $\pi \rightarrow \pi^*$ transition on the pyrazine ring, consistent with the original assignment. They also reported an intense absorption band in the visible range at about 470 nm, which they assigned to MLCT. This band contains multiple components, including the z-polarized $22A' \rightarrow 26A'$ (which may be thought of as a transition from bonding to antibonding combinations of Ru d_{xz} and ligand orbitals and is predicted at 420 nm). It also contains the uncoupled (i.e. not d_{xz}) t_{2g}-to-π^* (or t_{2g}-to-antibonding), predicted at 463 nm.

Table 6
Spectra of $[Ru(NH_3)_5pyz]^{2+}$ and $[Ru(NH_3)_5pyz]^{3+}$

Exp.		Calc.	
λ (nm)	Assignment	λ (nm)	Assignment
$[Ru(NH_3)_5pyz]^{2+}$			
250	$\pi \rightarrow \pi^*$	236	$\pi \rightarrow \pi^*(z)$
470	MLCT	420	$t_{2g} \rightarrow A(z)$
		463	$t_{2g} \rightarrow A(x)$
$[Ru(NH_3)_5pyz]^{3+}$			
238		237	$\pi \rightarrow \pi^*(z)$
270		282–328	$t_{2g} \rightarrow e_g(x, y, z)$
		324	$\pi \rightarrow t_{2g}(x)$

Table 7
Calculated transition operator energies for $[Ru(NH_3)_5pyz]^{2+}$ and $[Ru(NH_3)_5pyz]^{3+}$

Transition	ν (cm^{-1})	λ (nm)	Assignment	Pol.
$[Ru(NH_3)_5pyz]^{2+}$				
$22A' \rightarrow 26A'$	37200	236	$\pi \rightarrow \pi^*$	z
$25A' \rightarrow 28A'$	30200	330	$t_{2g} \rightarrow e_g$	z
$25A' \rightarrow 26A'$	21700	463	$t_{2g} \rightarrow \pi^*$	x
$24A' \rightarrow 26A'$	23800	420	$d_{xz} \rightarrow \pi^*$	z
$24A' \rightarrow 28A'$	31600	318	$d_{xz} \rightarrow e_g$	x
$24A' \rightarrow 19A''$	29400	340	$d_{xz} \rightarrow e_g$	y
$17A'' \rightarrow 19A''$	28800	347	$t_{2g} \rightarrow e_g$	x
$17A'' \rightarrow 28A'$	31200	320	$t_{2g} \rightarrow e_g$	y
$[Ru(NH_3)_5pyz]^{3+}$				
$22A' \rightarrow 26A'$	42200	237	$\pi \rightarrow \pi^*$	z
$22A' \rightarrow 25A'$	30900	324	$\pi \rightarrow t_{2g}$	x
$24A' \rightarrow 27A'$	30800	325	$d_{xz} \rightarrow d_{z2}$	x
$23A' \rightarrow 26A'$	29000	345	$t_{2g} \rightarrow \pi^*$	x
$23A' \rightarrow 27A'$	31400	320	$t_{2g} \rightarrow e_g$	z
$24A' \rightarrow 25A'$	381	26200	$d_{xz} \rightarrow t_{2g}$	x
$24A' \rightarrow 26A'$	27200	389	$d_{xz} \rightarrow \pi^*$	z
$24A' \rightarrow 18A''$	30500	328	$d_{xz} \rightarrow e_g$	y
$17A'' \rightarrow 18A''$	30800	325	$t_{2g} \rightarrow e_g$	x
$17A'' \rightarrow 25A'$	1070	9540	$d_{yz} \rightarrow d_{x2-y2}$	y
$17A'' \rightarrow 27A'$	35700	282	$t_{2g} \rightarrow e_g$	y

For the Ru(III) monomer Ford et al. reported two bands at 270 and 238 nm in a faintly yellow solution without assignment. We find a z-polarized $\pi \rightarrow \pi^*$ transition at 237 nm. There are a couple of possible assignments for the lower energy band. There is an x-polarized $\pi \rightarrow t_{2g}$ transition at 324 nm. There is also a series of $t_{2g} \rightarrow e_g$ transitions with x, y and z polarizations in the range 282–328 nm. This latter set of transitions is Laporte forbidden in O_h but allowed in C_{2v} symmetry. One also notices that the energy gap between the uncoupled t_{2g} orbitals and the 26A′ orbital is lower for Ru(II), 420 nm, than that for the Ru(III), 345 nm. This indicates a better energy match for backbonding for the Ru(II) complex.

Other possible transitions are listed in Table 7 for the 2+ and the 3+ species.

6. Comments on the asymmetric crown ether complexes

The electronic structure of pyrazine in an asymmetric environment has implications in another recent issue

in mixed-valence chemistry. Complexes of bridged mixed-valence compounds with crown ethers have been reported recently and exhibit unprecedented stoichiometry dependent spectroscopic features [18,19,35]. In particular, when the Creutz–Taube ion is complexed with a crown ether in a 1:1 crown:cation ratio, the intervalence band becomes substantially broader, blue-shifted and less intense. At a 2:1 crown:cation ratio, the original spectrum is nearly recovered [18]. The broad, blue-shifted band of the asymmetric 1:1 complex was attributed to either complete or partial valence delocalization. The present results offer some suggestions about the role of the bridging ligand in the intriguing spectroscopic behavior of the crown ether encapsulated dimeric species.

The LCAO coefficients for the 2+ (Table 4) and 3+ (Table 5) monomeric species show that the occupied π molecular orbitals (19A′, 22A′, 16A″ and 24A′ for the 2+ species and 20A′, 22A′, 16A″ and 24A′ for the 3+ species) are highly asymmetrical. Noting that the electron occupation numbers are proportional to the squares of the LCAO coefficients and comparing each of the four occupied orbitals in Table 4 with its corresponding orbital in Table 5, one finds that the electron occupation numbers for the π atomic basis orbitals of the pyrazine ligand are strongly dependent upon the charge on the adjacent metal ion. Therefore any transition involving asymmetric charge displacement between the two metal ions in a pyrazine-bridged binuclear species will also involve asymmetric charge displacement within the pyrazine ligand, and a number of antisymmetric vibrational modes of the pyrazine ring will be coupled to that transition.

If the 1:1 crown:cation complex is valence localized with a double well ground state, clearly antisymmetric modes of the pyrazine ring and metal ions will be coupled to the intervalence band. (In the Creutz–Taube ion and in the doubly encapsulated species, only totally symmetric modes are coupled to the intervalence band.)

However the high sensitivity of the pyrazine occupation numbers to the charge on the adjacent metal ion, as discussed above, indicates that there may be substantial coupling of the antisymmetric pyrazine modes to the intervalence transition, even if the ground state of the 1:1 crown:cation complex has single minimum form. This is because the small asymmetry between the coupled orbitals on the two Ru atoms (a few tenths of an eV [35]) in the 1:1 complex introduces some metal-to-metal charge-transfer character to the intervalence band.

The contributions of the antisymmetric pyrazine modes to the absorption lineshape in the 1:1 complex are difficult to calculate in the absence of experimentally measured vibronic coupling constants. On the other hand, the contributions of the symmetric and antisymmetric metal–ligand stretch modes and symmetric pyrazine modes may be easily estimated using the simple model Hamiltonian parameters reported previously [8], and in fact only account for a fraction of the observed linewidth in the 1:1 crown:cation complex.

7. Conclusions

Our HFS-DVM results show that the extent of mixing of the Ru d_{xz} orbital with the π and the π^* orbitals of pyrazine is dependent upon the charge of the complex, and consistent with the experimental work of Creutz and Chou. Mixing of the $4d_{xz}$ and π^* orbitals is strong in the 2+ complex and very weak in the 3+ complex. Mixing of the $4d_{xz}$ and π is weak in the 2+ complex and a little less weak in the 3+ complex. A cautionary note is in order here: because the D_{2h} symmetry of pyrazine is broken, the π and π^* orbitals of the free pyrazine molecule appear in heavily distorted form in the molecular orbitals of the present cations. Therefore these comments about mixing of π and π^* orbitals are not intended to be interpreted strictly.

Our transition operator calculations have confirmed the original [14] assignments of optical absorption transitions at 250 and 472 nm for $(NH_3)_5Ru(pyz)^{2+}$ and have suggested assignments for transitions observed at 238 and 270 nm for $(NH^3)_5Ru(pyz)^{3+}$.

The polarization of the pyrazine ligand was found to be toward the metal ion in both complexes, as a simple electrostatic model would predict.

It is interesting to note that the higher T_c ceramic superconductors are mixed-valence compounds joined together by the polarizable oxide bridges. The valence of the metal ions is 'tunable' through doping, and the critical temperature for superconductivity is a very sensitive function of the stoichiometry [36,37]. In order to understand these fascinating compounds, we must understand how the degree of the metal–ligand coupling depends upon the valence of the metal ion.

We find the dependence of the metal–ligand π-electron conjugation upon electron occupation in complexes of the type studied here to be very intriguing. In some instances, it is possible that increased resonance stabilization upon the addition of an electron could lead to interesting conductive properties [38,39]. These differences between the two species are attributed to different energy gaps caused by greater electron–electron repulsion in the 2+ species, and also to increases in the dipole moment and higher moments of the ligand in the 3+ species. It is possible that extended, periodic networks of such metal ions and bridging ligands may have conductive properties with potentially useful applications. The asymmetric distribution of electron density within the pyrazine ligand was found to be very sensitive to the charge on the neighboring metal ion. This supports the notion that,

if accurate vibronic coupling constants can be measured, asymmetric complexation may prove to be a very valuable probe in mixed-valence chemistry.

Acknowledgements

We thank the National Science Foundation for support of this research under Grant No. CHE-8820340. We are grateful to Professor Joe Hupp for valuable correspondence and for supplying us with results prior to their publication. M.J.O. thanks Professor Jan Linderberg and Dr Matthew D. Todd of Aarhus University, Aarhus, Denmark for valuable discussions. We thank Dr Xu Monica Wu and Messrs Saeed Gozashti, Ihsan Shehadi and Leonel Murga for their assistance.

References

[1] H. Taube, *Surv. Prog. Chem., 6* (1973) 1.
[2] K. Kalyanasundaram, *Coord. Chem. Rev., 45* (1982) 159.
[3] C. Creutz and H. Taube, *J. Am. Chem. Soc., 91* (1969) 3988; *95* (1973) 1086.
[4] U. Fürholz, H.B. Bürgi, F.E. Wagner, A. Stebler, J.H. Ammeter, E. Krausz, R.J.H. Clark and A. Ludi, *J. Am. Chem. Soc., 106* (1984) 121, and refs. therein.
[5] J.K. Beattie, N.S. Hush and P.R. Taylor, *Inorg. Chem., 15* (1976) 992.
[6] N.S. Hush, A. Edgar and J.K. Beattie, *Chem. Phys. Lett., 69* (1980) 128.
[7] L.T. Zhang, J. Ko and M.J. Ondrechen, *J. Am. Chem. Soc., 109* (1987) 1666.
[8] M.J. Ondrechen, J.Ko and L.T. Zhang, *J. Am. Chem. Soc., 109* (1987) 1672.
[9] K. Neuenschwander, S.B. Piepho and P.N. Schatz, *J. Am. Chem. Soc., 107* (1985) 7862.
[10] D.H. Oh and S.G. Boxer, *J. Am. Chem. Soc., 112* (1990) 8161–8162.
[11] A. von Kameke, G.M. Tom and H. Taube, *Inorg. Chem., 17* (1978) 1790.
[12] X.M. Wu and M.J. Ondrechen, *Chem. Phys. Lett., 205* (1993) 85–90.
[13] M. Hanack, *Israel J. Chem., 25* (1985) 205.
[14] A.M. Zwickel and C. Creutz, *Inorg. Chem., 10* (1971) 2395.
[15] P.C. Ford, De F.P. Rudd, R. Gaunder and H. Taube, *J. Am. Chem. Soc., 90* (1969) 1187.
[16] M.E. Gress, C. Creutz and C.O. Quicksall, *Inorg. Chem., 20* (1981) 1522.
[17] C. Creutz and M.H. Chou, *Inorg. Chem., 26* (1987) 2995.
[18] Y. Dong, D. Yoon and J.T. Hupp, *J. Am. Chem. Soc., 115* (1993) 4379.
[19] J.T. Hupp and Y. Dong, submitted for publication.
[20] C. Creutz, *Prog. Inorg. Chem., 30* (1983) 1.
[21] M. Tanner and A. Ludi, *Inorg. Chem., 20* (1981) 2348.
[22] M.J. Ondrechen, D.E. Ellis and M.A. Ratner, *J. Am. Chem. Soc., 103* (1981) 1656.
[23] M.J. Ondrechen, D.E. Ellis and M.A. Ratner, *Chem. Phys. Lett., 109* (1984) 50.
[24] W.J. Pietro, D.E. Ellis, T.J. Marks and M.A. Ratner, *Mol. Cryst. Liq. Cryst., 105* (1984) 273.
[25] F.W. Kutzler, P.N. Swepston, Z. Berkovitch-Yellin, D.E. Ellis and J.A. Ibers, *J. Am. Chem. Soc., 105* (1983) 2996.
[26] J.C. Slater, *Quantum Theory of Molecules and Solids,* Vol. 4, McGraw-Hill, New York, 1974.
[27] D.E. Ellis, *Int. J. Quantum Chem., IIS* (1968) 35.
[28] C.B. Haselgrove, *Math. Computation, 15* (1961) 323.
[29] E.J. Baerends and P. Ros, *Int. J. Quantum Chem., Symp., 12* (1978) 169.
[30] R.S. Drago, *Physical Methods in Chemistry,* Sanders, Philadelphia, PA, 1977.
[31] P.S. Sun, M.S. Shao and C.L. Gu, *Acta Energ. Sol. Sinica, 4* (1983) 163; R. Benedix and H. Hennig, *J. Prakt. Chem.,* (1984) 962–970.
[32] B. Folkesson, *Acta Chem. Scand., 26* (1972) 4008; *27* (1973) 276.
[33] J.N. Murrell, A. Al-Derzi, G.J. Leigh and M.F. Guest, *J. Chem. Soc., Dalton Trans., 8* (1980) 425.
[34] R. Hoffman, M.M.C. Chen and D.L. Thorn, *Inorg. Chem., 16* (1977) 503.
[35] M.D. Todd, Y. Dong and J.T. Hupp, *Inorg. Chem., 30* (1991) 4685–4687.
[36] R.J. Cava, B. Batlogg, C.H. Chen, E.A. Rietman, S.M. Zahurak and D. Werder, *Nature (London), 329* (1987) 423.
[37] A.W. Sleight, *Science, 242* (1988) 1519.
[38] M.J. Ondrechen, S. Gozashti and X.M. Wu, *J. Chem. Phys., 96* (1992) 3255–3261.
[39] A. Ferretti and A. Lami, *Chem. Phys., 181* (1994) 104.